# *Ab initio* potential-energy surfaces for $Cd(^1P)+H_2 \Rightarrow CdH(X\,^2\Sigma^+)+H$, $HCdH(X\,^1\Sigma_g^+)$, $Cd(^3P)+H_2$, and $Cd(^1S)+H+H$

Jerry A. Boatz,[a] Maciej Gutowski, and Jack Simons[b]
*Department of Chemistry, University of Utah, Salt Lake City, Utah 84112*

(Received 20 December 1991; accepted 30 January 1992)

The outcome of laser excitation of the van der Waals $CdH_2$ complex [which consists of a ground-state $Cd(^1S)$ atom bound to an $H_2$ molecule] to its lowest-energy singlet state(s), which connects with $Cd(^1P) + H_2$, is examined by calculating *ab initio* potential-energy surfaces for the above excited singlet states, the corresponding underlying triplet states [connecting to $Cd(^3P) + H_2$], and the singlet ground state. It is necessary to study such a multitude of states because energetically accessible reaction products such as $Cd(^3P) + H_2$, $CdH(X\,^2\Sigma^+) + H$, Cd + H + H, and $HCdH(X\,^1\Sigma_g^+)$ connect to various surfaces. In carrying out these calculations, the lowest-energy surface of $^1A_1$ symmetry was evaluated at nearly 1100 $C_{2v}$ geometries using complete-active-space self-consistent-field wave functions with a valence double-zeta and a double-zeta-plus-polarization basis set on cadmium and hydrogen, respectively. The excited singlet and triplet surfaces that correlate with $^1P_1$ and $^3P_J$ levels of Cd plus ground-state $H_2$ were examined in detail along paths that flux prepared by laser excitation of the singlet surface(s) is most likely to follow. Among the photoexcited singlet states, the $^1B_2$ surface is found to provide the most energetically attractive approach path for the excited $CdH_2$ van der Waals complex to access geometries from which HCdH, Cd + H + H, and CdH + H can be formed via intersection and coupling with the lowest $^1A_1$ surface. The $^1B_1$ surface is found to be weakly attractive, and the excited $^1A_1$ surface to be repulsive at geometries characteristic of the nascent photoexcited species. The underlying triplet surfaces are found to be repulsive ($^3A_1$), weakly attractive ($^3B_1$), and slightly more attractive ($^3B_2$) at such geometries. The repulsive $^3A_1$ surface intersects the $^1B_2$ surface in the latter's entrance-channel "streambed"; the $^3B_1$ state intersects the $^1B_2$ surface closer to where the $^1B_2$ and lowest $^1A_1$ cross. The $^3A_1$ and $^1B_1$ surfaces also intersect in the entrance streambed of the latter. All such triplet–singlet crossings provide paths to $Cd(^3P) + H_2$.

## I. INTRODUCTION

### A. van der Waals "half-collision" experiments

The synthesis and excited-state chemistry of metal–rare-gas and similar metal–molecule van der Waals complexes have been topics of both experimental[1-12] and theoretical[13-19] studies for at least a decade. "Half-collision" experiments[1-9] in which a ground-state van der Waals complex is prepared and then promoted to an upper electronic state via photon excitation have yielded much structural, energetic, and reactivity information on low-lying excited-state potential-energy surfaces of several such molecules. For example, pump-and-probe laser experiments[5,8,9] have detected the electronic quenching of excited singlet-state Cd–Q complexes (Q is a quenching moiety, such as Xe, $H_2$, or $CH_4$) to produce triplet states that predissociate to yield $^3P_J$ Cd atoms and ground-state Q species.

Of particular importance for interpreting the $Cd + H_2$ experiments treated here are (i) the ground-state potential surface for geometries ranging from the van der Waals complex to those characterizing any and all product species, (ii) the low-energy excited states of the same spin multiplicity as the ground state over this same range of geometries, and (iii) the "close approach" or intersection of any underlying states of different spin multiplicity with any of these former states. For example, it is via such intersections that $^3P_J$ Cd atoms are thought to form in the above illustration.

### B. Using $H_2$ as a quencher for $Cd(^1P_1)$

Earlier "full-collision" experiments[10-12] in which $^1P$ Cd or $^3P_J$ Cd atoms are prepared and allowed to collide with quencher gas atoms or molecules provide data that supplements that obtained in the half-collision pump-and-probe experiments. When the hydrogen molecule is used as a potential quencher for $^1P_1$ Cd atoms in full-collision experiments, in addition to observing electronically deactivated $^3P_J$ Cd atoms (presumably generated via the intersection of a repulsive triplet surface correlating with the $^3P_J$ Cd atom + $H_2$ and one of the nascently excited singlet surfaces), the chemical reaction products CdH + H and Cd + H + H are also detected.[10] When $Cd(^3P_1)$ collides with $H_2$ (or $D_2$ or HD), $CdH(X\,^2\Sigma^+)$ (or CdD) is observed.[11,12] The rotational quantum state populations of the CdH (or CdD) are bimodal, and have been explained in terms of a small activation barrier on the triplet surface. The mechanisms by which all of the above reaction products are formed are the central focus of the work discussed here.

[a] Present address: Phillips Laboratory, Astronautical Sciences Division, Edwards Air Force Base, CA 93523.
[b] Corresponding author.

### C. The physical nature of the ground and lowest triplet and singlet-state surfaces of $CdH_2$ near the van der Waals complex geometry

#### 1. The ground-state van der Waals complex geometry

The chemically reactive events in the laser-excited half-collision experiments are thought to begin via excitation of ground-state singlet $CdH_2$ at a geometry characteristic of this weakly bound van der Waals complex. The complex is undoubtedly quite "floppy" with regard to angular motion of the $H_2$ moiety, but is thought to have an equilibrium structure with an H–H distance $r$ of ca. 0.76 Å and a Cd-to-center of H–H bond distance $R$ of ca. 4 Å. It is quite likely that "bending" motion of the $H_2$ moiety permits this complex to access linear or nearly linear geometries, as well as $C_{2v}$ or near $C_{2v}$ symmetries.

Therefore, we are required to explore the outcomes of photoexcitation processes that place the $CdH_2$ species on excited electronic states at geometries ranging from linear to $C_{2v}$. As shown below, flux that begins near linear geometries is less likely to progress toward any of the reaction products studied here because all excited singlet surfaces are repulsive for near-linear geometries. On the other hand, flux placed on excited-state singlet surfaces near $C_{2v}$ geometries (with $R$ near 4 Å and $r$ near 0.76 Å) is shown to experience attractive forces for the $^1B_2$ and $^1B_1$ states, which causes flux moving initially on these states to dominate the formation of the reaction products.

#### 2. The lowest excited singlet states

The $CdH_2$ complex has three ($^1A_1$, $^1B_1$, and $^1B_2$ in $C_{2v}$ geometry or $^1\Sigma$ and $^1\Pi$ for linear geometry) excited singlet states that derive from $^1P_1$ excited Cd interacting with a ground-state $H_2$ molecule. At the geometry of the ground-state van der Waals complex, these states *lie ca.* 125 *kcal/mol above the ground state* (our reference point of energy throughout this study). These singlet states have more than enough energy to produce $Cd(^3P) + H_2$ (which lies at 88 kcal/mol), HCdH (which lies at 24 kcal/mol), $Cd(^1S) + H + H$ (lying at 110 kcal/mol), or $CdH(X\,^2\Sigma^+) + H$ (at 92 kcal/mol). They do *not* have enough energy to generate excited $CdH(A\,^2\Pi) + H$ (at 157 kcal/mol) or $CdH(B\,^2\Sigma^+) + H$ (at 163 kcal/mol). These and other *relevant energies are summarized in* Table I; all such energies do not contain any zero-point corrections.

Near the geometry of the ground-state van der Waals complex, the three singlet states are expected to display quite different behaviors as functions of $R$, the distance from the Cd atom to the midpoint of the H–H bond. Our findings indeed detect such differences, and show that the most energetically favorable approach for nascently excited $CdH_2$ is along $C_{2v}$ symmetry (or nearly so), with the $^1B_2$ surface being the most attractive, and the $^1B_1$ surface weakly attractive. Linear approaches or approach on the $^1A_1$ surface at near $C_{2v}$ symmetry are not favorable in the van der Waals region.

#### 3. The lowest excited triplet states

The $CdH_2$ complex has three ($^3A_1$, $^3B_1$, and $^3B_2$ in $C_{2v}$ geometry or $^3\Sigma$ and $^3\Pi$ for linear geometry) excited triplet states that derive from $^3P_J$ excited Cd interacting with a ground-state $H_2$ molecule. At the geometry of the ground-state van der Waals complex, these states lie *ca.* 88 *kcal/mol above the ground state.* The primary relevance of these triplet states to the present study is that they provide, by their inter-

TABLE I. Structures and relative energies of various states of $CdH_2$, $Cd + H_2$, HCdH, and $CdH + H$.[a]

| Species | Geometry[b] (Å) | Calc. energy (kcal/mol)[b] | Expt. energy (kcal/mol) |
|---|---|---|---|
| $Cd(^1S) + H_2$ | $R = \infty, r = 0.76$ | 0 | 0 |
| $Cd(^3P) + H_2$ | $R = \infty, r = 0.76$ | 78 | 88[c] |
| $Cd(^1P) + H_2$ | $R = \infty, r = 0.76$ | 126 | 125[c] |
| $Cd(^1S) + H + H$ | $R = \infty, r = \infty$ | 96 | 110[d] |
| $CdH(X\,^2\Sigma^+) + H$ | $R_{CdH} = 1.83$ | 85 | 92[d] |
| $CdH(A\,^2\Pi) + H$ | $R_{CdH} = 1.76$ | 148 | 157[d] |
| $CdH(B\,^2\Sigma) + H$ | $R_{CdH} = 2.51$ | 151 | 163[d] |
| $HCdH(^1\Sigma_g^+)$[e] | $R = 0.0, r = 3.48$ | 24 | |
| $CdH_2(^1B_2)$[e] | $R = 1.69, r = 1.92$ | 106 | |
| $CdH_2(^3B_2)$[e] | $R = 1.70, r = 2.12$ | 86 | |
| $CdH_2(^1A_1)$[f] | $R = 1.69, r = 1.92$ | 99 | |
| $CdHH(^3\Sigma^+)$[g] | $R = 2.56, r = 1.16$ | 106 | |
| $CdH_2(^3B_2)$[h] | $R = 1.84, r = 1.28$ | 92 | |

[a] All energies in kcal/mol relative to $Cd(^1S) + H_2$; no zero-point corrections are included.
[b] This work.
[c] Reference 26.
[d] Reference 27.
[e] The energies and geometries reported correspond to the local equilibrium geometries of these species on the electronic state specified.
[f] This energy belongs to the *ground* $^1A_1$ state at the geometry where the $^1B_2$ state has its minimum. The 99 and 106 kcal/mol demonstrate that the $^1B_2$ state lies above the $^1A_1$ state at this geometry.
[g] This point is a transition state on the colinear $Cd(^3P) + HH \Rightarrow CdH(X\,^2\Sigma^+) + H$ surface.
[h] This point is a transition state on the $Cd(^3P) + H_2 \Rightarrow CdH_2(^3B_2)$ surface.

section(s) with the laser-accessed singlet states, the primary route to $Cd(^3P_J) + H_2$ and one of two routes to $CdH(X\,^2\Sigma^+) + H$.

Near the geometry of the ground-state van der Waals complex, the three triplet states are also expected to display quite different behaviors as functions of $R$. Our findings detect such differences, and show that the most repulsive interaction arises from the $^3A_1$ surface. The $^3B_1$ and $^3B_2$ surfaces are weakly attractive at such geometries.

### D. Why emphasis is placed on $C_{2v}$ geometries

In attempting to address the fate of flux prepared via photon absorption on the three singlet excited surfaces, we can ignore flux that is prepared near linear geometries. At such geometries all three singlet states ($2\,^1\Sigma^+$ and $^1\Pi$) are either repulsive ($2\,^1\Sigma^+$) or not nearly as attractive ($^1\Pi$) as for $C_{2v}$ geometries (see Sec. III B). Thus, flux prepared near linear geometries will either (i) move outward to larger $R$ values ($2\,^1\Sigma^+$) or (ii) "wait" ($^1\Pi$) until bending motion causes the complex to access near-$C_{2v}$ geometries at which time it will encounter strongly attractive forces that move it to smaller $R$.

For these reasons, the three singlet PESs (potential-energy surfaces) were examined by performing $C_{2v}$-symmetry calculations beginning near the ground-state van der Waals complex geometry $R = 4$ Å and $r = 0.76$ Å. For these PESs, gradient information was employed to search for minima and transition states as well as to find and follow "streambeds" that connect such stationary points. The stabilities of $C_{2v}$ geometries to asymmetric distortions of $b_2$ symmetry were tested at various points along the streambeds.

In addition to mapping out the most energetically favorable directions for flux to flow on the singlet PESs (in particular, the $^1B_2$ and $^1B_1$ surfaces), cognizance was taken of the locations of nearby triplet states as "streambeds" were followed on these *singlet* surfaces. Any intersections of the singlet-state surface being followed by underlying triplet surface(s) were noted; such intersections are of great importance because they provide access to $Cd(^3P) + H_2$ products.

### E. The role of the underlying ground-state $^1A_1$ surface

#### *1. The ground-state HCdH and Cd+H+H species lie on the underlying $^1A_1$ surface*

As reaction flux begins to evolve on the $^1B_2$ surface under the $C_{2v}$ geometries characteristic of the "insertion" path described briefly above, strong forces arise that cause the $CdH_2$ nuclei to move to smaller $R$ values and to somewhat larger H–H distances ($r$) while preserving $C_{2v}$ symmetry. Eventually, the $^1B_2$ surface approaches and intersects the $^1A_1$ surface, whose energy rises along this path because of the Woodward–Hoffmann "forbidden" nature of the ground-state $Cd + H_2$ insertion reaction.[15,17] Production of *ground-state* HCdH, which lies on the underlying $^1A_1$ PES, can thus occur if flux can evolve onto this $^1A_1$ surface from the $^1B_2$ surface. Possible mechanisms for such $^1B_2$-to-$^1A_1$ surface "hoppings" are therefore important topics that the present work needs to address.

It turns out that the $^1B_1$ surface does *not* approach the $^1A_1$ surface along a path that flux would follow if placed on it, so $^1B_1$–$^1A_1$ PES "hoppings" do not provide an avenue to HCdH formation.

#### *2. Intersections or nonadiabatic couplings between the $^1B_2$ and $^1A_1$ surfaces can open the HCdH($X\,^1\Sigma^+$) and Cd($^1S$)+H+H channels*

As flux evolves on the $^1B_2$ surface along $C_{2v}$ symmetry, geometries may be reached near which the $^1B_2$ and $^1A_1$ surfaces intersect. At such geometries, even slight asymmetric distortions of the $CdH_2$ framework can cause flux to be "funnelled" to the $^1A_1$ surface. Such distortions reduce the symmetry from $C_{2v}$ to $C_s$ under which the $^1A_1$ and $^1B_2$ surfaces both are of $^1A'$ symmetry and hence can couple.

Once on the $^1A_1$ surface, the HCdH and Cd + H + H products may be formed since the energy of the initially excited $^1B_2$ state of $CdH_2$ makes both product channels accessible. Only the presence of a substantial activation barrier along the paths to these products would alter this conclusion.

#### *3. Intersections and nonadiabatic couplings between the $^1B_2$ and $^1A_1$ surfaces can also lead to CdH($X\,^2\Sigma^+$)+H*

The above surface-intersection picture can also explain how the asymmetric reaction products CdH + H can be formed. If $C_{2v}$ symmetry were rigorously retained, CdH + H could not be formed by flux that exists on either surface ($^1B_2$ or $^1A_1$) even if the surfaces intersect. However, if distortions away from $C_{2v}$ geometries occur (as they must because of the zero-point motion along the asymmetric $b_2$ vibration of $CdH_2$), flux can evolve from one surface to the other near their intersections. Once non-$C_{2v}$ symmetry is reached, the path to $CdH(^2\Sigma^+) + H$ (lying at 92 kcal/mol) may be available. The CdH + H path is likely to be followed unless strong restoring forces (i.e., large positive curvature) exist along the $b_2$ mode direction. For this reason, in the present work the curvature along the $b_2$ direction has been monitored for the $^1B_2$ and $^1A_1$ surfaces; in either case, the appearance of negative curvature provides a sign of geometrical instability that may lead to CdH + H.

In addition to the possibility that the surfaces intersect and thereby cause flux to move from the $^1B_2$ to the $^1A_1$ surface, there exists a mechanism that does not require surface intersection. Nonadiabatic coupling, induced by vibrational motion along the asymmetric $b_2$ vibration of $CdH_2$, can also couple the $^1B_2$ and $^1A_1$ surfaces. Such couplings are known[20] to occur most strongly when the two surfaces involved approach closely in energy, but surface intersection is *not* necessary. To explore the role of this mechanism, it is again important to locate geometries at which the two states approach closely and to monitor the curvatures of the two PESs along the $b_2$ direction.

### F. Asymmetric-mode instability is the key to forming CdH($X\,^2\Sigma^+$)+H

Formation of the asymmetric reaction products CdH + H requires that geometrical instability exist along the asymmetric distortion mode somewhere along the path taken by the reaction flux. Since the flux is assumed to begin on the $^1B_2$ surface, it is natural to first search for geometries at which instability along the $b_2$ distortion mode appears on this surface. If such geometries do not exist or are energetically unaccessible, the $^1A_1$ surface should be searched for such unstable geometries because flux can eventually move to this surface from the $^1B_2$ surface as discussed above. If such instability occurs while the flux is on the $^1A_1$ surface, this flux can move spontaneously away from $C_{2v}$ symmetry and thus toward CdH + H; if instability occurs while on the $^1B_2$ surface, the flux can move toward CdH + H while on this surface.

The strength of the factors that produce negative $b_2$-mode curvature on, for example, the $^1A_1$ surface is governed by matrix elements of the form[20]

$$\frac{|\langle {}^1A_1|\partial H/\partial Q_{b_2}|{}^1B_2\rangle|^2}{E({}^1A_1)-E({}^1B_2)},$$

where $\partial H/\partial Q_{b_2}$ represents the derivative of the electronic Hamiltonian with respect to distortion along the $b_2$ mode. The closer the $^1B_2$ state approaches the underlying $^1A_1$ state, the larger is the magnitude of this $^1A_1$-state negative-curvature factor. Only at geometries where the $^1B_2$ state lies *above* the $^1A_1$ state will negative $b_2$ curvature likely to occur on the $^1A_1$ PES.

Alternatively, the $^1B_2$ state may develop negative $b_2$ curvature if the $^1B_2$ state intersects and moves below the $^1A_1$ state. In this case, the same factor displayed above, but with opposite sign, induces negative $b_2$-mode curvature on the $^1B_2$ state. In either event, *one* of the two states (*the lower-energy PES* at any geometry) may possess instability along the asymmetric $b_2$ mode, and therefore provide an open channel to production of CdH + H products. To explore these possibilites, one must search for geometries at which the two electronic states intersect or approach closely; clearly, this became one of the primary tasks of the present work.

### G. Formation of Cd($^3P$)+$H_2$ involves intersections by underlying triplet surfaces

As flux moves inward to smaller $R$ values either on the (strongly attractive) $^1B_2$ surface or on the (weakly attractive) $^1B_1$ surface, repulsive triplet-state surfaces may approach and intersect the singlet surface from below. In this event, flux can "hop" (albeit, with spin–orbit coupling required) to the triplet surface, and subsequently lead to Cd($^3P_J$) + $H_2$ products. Such intersections have indeed been found for both of the above singlet surfaces and are characterized in Sec. III C.

## II. COMPUTATIONAL METHODS

### A. Configuration space

In order to obtain a qualitatively accurate description of the global $^1A_1$ potential-energy surface for $CdH_2$, complete-active-space self-consistent-field (CASSCF) wave functions were employed. The active space consisted of the two 5*s* electrons of Cd and the two $\sigma_g$ electrons of $H_2$ distributed in all possible ways among the six valence orbitals. In the asymptotic region corresponding to Cd + $H_2$, these orbitals are the 5*s* and 5*p* orbitals of Cd and the $\sigma_g$ and $\sigma_u^*$ orbitals and $H_2$. For $C_{2v}$ geometries in which the Cd and $H_2$ moieties interact, they are three $a_1$, one $b_1$, and two $b_2$ orbitals. At linear geometries, using the $C_{2v}$ symmetry limits of our computer codes, these are four $a_1$ (i.e., $\sigma$), one $b_1$ (i.e., $\pi$), and one $b_2$ (i.e., $\pi$) orbitals.

Preliminary calculations which included the outermost occupied *d* orbitals of Cd in the active space showed that they were of minor importance in describing the addition of $H_2$ to Cd on the $^1A_1$ PES. For example, the natural orbital occupation numbers of the *d* orbitals were consistently greater than 1.99 electrons; hence, they were excluded from the active space in the large number of calculations needed to describe the PES studied here.

This choice of active space yields 37 and 28 configuration state functions (CSFs) of $^1A_1$ and $^1B_2$ symmetry, respectively, and is sufficiently flexible to describe the asymptotic Cd + $H_2$, Cd + H + H, and linear H–Cd–H regions of the potential-energy surface, the Cd($^1S$) + $H_2$ and Cd($^1P$) + $H_2$ linear species, as well as all intermediate points. While a more extensive treatment of correlation as well as consideration of spin–orbit coupling would be required to obtain quantitative accuracy in the surface, the present CASSCF treatment is sufficient for qualitative interpretations of the PES.

### B. Atomic-orbital basis sets

The basis set used for cadmium consists of the Hay–Wadt effective core potential and the associated valence double-zeta basis set.[21] In order to obtain a more accurate $^1S \rightarrow {}^1P$ excitation energy for Cd, a set of diffuse *s* and *p* functions were added to the valence basis set, with exponents of 0.021 76 and 0.0162, respectively. The basis set for hydrogen was constructed by adding a set of *p*-type polarization functions (with an exponent of 1.1) to the Pople -21 G hydrogen basis.[22]

All calculations were performed using GAMESS (Ref. 23) or the MESSKIT (Ref. 24) suite of computer programs. The $^1A_1$ PES was constructed by calculating a grid of approximately 1100 single-point energies, which were then fit using a two-dimensional cubic spline interpolation.

### C. Geometrical curvature calculations

As explained in the Introduction, it is anticipated that some regions of the ground $^1A_1$ or excited $^1B_2$ PES will be energetically unstable with respect to distortions of $b_2$ symmetry (i.e., the asymmetric Cd–H stretch). In order to determine the regions of the surface in which this occurs, the matrix of energy second derivatives (i.e., the Hessian ma-

trix) was computed at selected points. Neither GAMESS nor our MESSKIT program can carry out such a second-derivative calculation analytically with the pseudopotentials employed for Cd, so finite-difference methods were used to compute the second energy derivative from the analytically calculated first derivatives. This was followed by application of the projection scheme of Miller, Handy, and Adams[25] (to project out the nonzero gradient vector) and diagonalization to determine if the $b_2$ mode has an imaginary frequency.

### D. Geometries to explore

Points of the $^1B_2$ PES were computed (1) near the ground-state van der Waals complex geometry that characterizes the nascent photoexcited species of the half-collision experiments, (2) along a "streambed" path connecting this initially excited $^1B_2$ species with the 20 kcal/mol deep minimum on this same $^1B_2$ surface (this path is detailed later), (3) in regions where the ground $^1A_1$ surface displayed negative curvature along the asymmetric stretching mode of $b_2$ symmetry (such regions signal the close approach of the $^1B_2$ PES), (4) in regions where the $^1B_2$ and $^1A_1$ PESs intersect, and (5) along the above $^1B_2$ state's streambed where intersections with $^3A_1$ and $^3B_1$ PESs were detected.

Points on the ground $^1A_1$ surface were evaluated at a large number of $R$ and $r$ values to achieve a more global picture. Moreover, efforts were made to find and characterize geometries at which $b_2$-mode instability is present on the $^1A_1$ surface as well as geometries where the $^1B_2$ surface intersects this $^1A_1$ surface.

The $^1B_1$ PES was examined (1) near the ground-state van der Waals complex geometry that characterizes the nascent photoexcited species of the half-collision experiments, (2) along its own streambed path in which $R$ is varied from ca. 4 Å inward to 1.6 Å with $r$ "optimized" to produce the minimum $^1B_1$ energy for each such $R$ value [this path describes qualitatively how flux would most probably evolve if placed on the (weakly attractive) $^1B_1$ surface], and (3) along this same $^1B_1$ path, focusing on where an intersection with the $^3A_1$ state is detected in the entrance valley.

## III. RESULTS AND DISCUSSION

### A. Calibration of calculated results

A feel for the accuracy with which the basis sets and *ab initio* methods used here reproduce experimental energies was obtained by calculating the $^1S \rightarrow {}^{1,3}P$ atomic excitation energies of cadmium and the bond dissociation energy $D_e$ of the hydrogen molecule. In addition, *ab initio* calculations were performed for the $X\,^2\Sigma^+$, $A\,^2\Pi$, and $B\,^2\Sigma^+$ states of CdH. For the excitation energies, the calculated values of 125.9 and 78.4 kcal/mol can be compared with the experimental values of 124.9 and 87.6 kcal/mol.[26] Because the relative positions of singlet and triplet surfaces that derive from the $^{1,3}P$ levels of Cd are of utmost importance, we later must consider the effects of "shifting" our calculated triplet-state surfaces upward by $87.6 - 78.4 = 9$ kcal/mol to achieve better representations of these relative energies.

The calculated $H_2$ well depth of 96.0 kcal/mol is somewhat smaller than the experimental $D_e$ value of 109.5 kcal/mol,[27] again by an amount that is not entirely satisfactory. The calculated vibrational frequencies ($^{114}$Cd $^1$H) for the $X\,^2\Sigma^+$, $A\,^2\Pi$, and $B\,^2\Sigma^+$ states of CdH 1278, 1428, and 895 $cm^{-1}$, respectively, qualitatively reproduce the experimental values[27] 1337, 1700, and 1000 $cm^{-1}$. A prior theoretical relativistic computation[28] of the geometry of the linear H–Cd–H molecule gave a Cd–H bond length of 1.733 Å, which is in very good agreement with our calculated value of 1.741 Å. All of the *relevant energies* obtained for stable species $Cd(^1S, {}^{1,3}P) + H_2$, $HCdH(^1\Sigma_g^+)$, $CdH_2$ ($^1A_1$, $^1B_2$, $^3B_2$), $H + Cd + H$, and $CdH(X\,^2\Sigma^+, B\,^2\Sigma^+$, and $A\,^2\Pi) + H$ are *summarized in Table I.*

### B. Long-range interaction energies relevant to the van der Waals region

To estimate the large-$R$ (i.e., van der Waals region) interaction energies of the various states that arise from $^1P$ Cd or $^3P$ Cd interacting with $H_2$, we performed the following calculations:

(i) We used the same six-orbital CASSCF procedure used to map out all of the potential surface features reported here to compute the energies of ground $^1A_1$, and excited $^{1,3}A_1$, $^{1,3}B_1$, and $^{1,3}B_2$ $CdH_2$ all for $r = 0.76$ Å (the equilibrium bond length of $H_2$) and $R = 50$ Å (i.e., essentially infinitely far away). These energies are reported in Table II.

(ii) In each such calculation, we allowed the six valence orbitals to be optimized to produce the lowest total energy for the state under study. The physical natures of these valence orbitals are also given in Table II.

(iii) We then calculated the energies of these same $^1A_1$, $^{1,3}A_1$, $^{1,3}B_1$, and $^{1,3}B_2$ states at $R = 4.4$ Å, $r = 0.76$ Å, the presumed geometry of the ground-state van der Waals complex.

(iv) At the van der Waals geometry, we also employed the Boys and Bernardi[29] counterpoise method to calculate the basis-set superposition errors (BSSE) for each of the seven states. These errors ranged from 0.13 to 0.19 kcal/mol.

TABLE II. Relative energies of $CdH_2$ species used to evaluate long-range interaction energies.[a]

| Species | Nature of six valence orbitals | Calc. energy (kcal/mol)[b] |
|---|---|---|
| $CdH_2$ ($1\,^1A_1$) | $5s,5p,\sigma_g,\sigma_u$ | 0 |
| $CdH_2$ ($2\,^1A_1$) | $5s,5p_y,5p_z,$ $\sigma_g,\sigma_u,\pi_x$ | 123 |
| $CdH_2$ ($^1B_1$) | $5s,5p_x,1\sigma_g,$ $1\sigma_u,2\sigma_g,2\sigma_u$ | 121 |
| $CdH_2$ ($^1B_2$) | $5s,5p_y,1\sigma_g,$ $1\sigma_u,2\sigma_g,\pi_x$ | 119 |
| $CdH_2$ ($^3A_1$) | $5s,5p_z,1\sigma_g,$ $1\sigma_u,2\sigma_u,\pi_x$ | 75 |
| $CdH_2$ ($^3B_1$) | $5s,5p_x,1\sigma_g,$ $1\sigma_u,2\sigma_g,2\sigma_u$ | 73 |
| $CdH_2$ ($^3B_2$) | $5s,5p_y,1\sigma_g,$ $1\sigma_u,2\sigma_g,\pi_x$ | 71 |

[a] All energies in kcal/mol relative to $Cd(^1S) + H_2$.

[b] As calculated in this work.

(v) By subtracting from our BSSE-corrected energies at $R = 4.4$ Å, $r = 0.76$ Å our $R = 50$ Å, $r = 0.76$ Å energies, we obtain an estimate of the interaction energies for the seven electronic states.

These *results are* given in Table III and are *summarized qualitatively* in Fig. 1(a). In Table III, we also show the interaction energies that would obtain if one were to include only the quadrupole–quadrupole interactions between $H_2$ and the various states of Cd. These data show clearly that the $^{1,3}A_1$ states' interaction energies are *not* entirely quadrupole–quadrupole at these geometries (repulsions due to orbital overlaps are present), but the $^{1,3}B_{1,2}$ have strong or even dominant quadrupole–quadrupole components here.

Our CASSCF wave function contains no configurations capable of describing dispersion interactions among $H_2$ and the various states of Cd. Our wave functions are capable of describing the dominant (because it varies as $R^{-5}$) long-range electrostatic interaction deriving from the quadrupole moment of $H_2$ interacting with the quadrupole moments of the various states of Cd. For these reasons, our interaction energies can be considered as reasonable at large $R$, but subject to increased attractions amounting to $<2$ kcal/mol (due to dispersion) as $R$ decreases, with the largest such corrections thus arising at small $R$.

The data of Table III show the following in the van der Waals region: (i) the *excited* $^{1,3}A_1$ *surfaces are repulsive* (by amounts that are not likely to be reversed when dispersion is included), (ii) the $^{1,3}B_2$ *surfaces are more attractive than the* $^{1,3}B_1$ *surfaces*, and (iii) the singlet surfaces are more attractive than their corresponding triplet surfaces (due to the larger quadrupole moments of $^1P$ Cd). In Fig. 1(a), the behavior of these states in the van der Waals region is denoted by the $R > 3$ Å region.

In the same fashion, we determined the CASSCF interaction energies for the $2\,^1\Sigma^+$ and $^1\Pi$ colinear states in the van der Waals region ($r = 0.76$ Å and $R = 4.4$ Å). We found that the $2\,^1\Sigma^+$ *surface is strongly repulsive* (3.19 kcal/mol) despite its attractive quadrupole–quadrupole interaction ($-0.65$ kcal/mol). As in the case of the $^{1,3}A_1$ states, the repulsive overlap effects dominate in the region where the photoexcitation places the $CdH_2$ species on the $2\,^1\Sigma^+$ surface.

The interaction energy for $^1\Pi$ *state* is also found to be *repulsive* (0.13 kcal/mol) as is the quadrupole–quadrupole interaction energy (by 0.32 kcal/mol). As with the $^1B_{1,2}$ states, the remaining components of the $^1\Pi$ state's interaction energy stabilize the complex.

In view of the repulsive interactions for the colinear complexes, the remainder of our study was focused on the attractive $C_{2v}$ $^1B_1$ and $^1B_2$ surfaces.

TABLE III. CAS-SCF interaction energies[a] $\Delta E$.

| State | $1\,^1A_1$ | $2\,^1A_1$ | $^1B_1$ | $^1B_2$ | $^3A_1$ | $^3B_1$ | $^3B_2$ |
|---|---|---|---|---|---|---|---|
| $\Delta E$[b] | 0.11 | 3.45 | −0.17 | −0.38 | 1.06 | −0.03 | −0.11 |
| $\Delta E$[c] | 0.0 | 0.31 | −0.08 | −0.24 | 0.14 | −0.04 | −0.11 |

[a] In kcal/mol determined at $R = 4.4$ Å, $r = 0.76$ Å in $C_{2v}$ geometry.

[b] From our *ab initio* quantum calculations.

[c] Pure quadrupole–quadrupole interaction for $Cd(^{1,3}P) + H_2$ computed as $Y(\Theta_{Cd}\Theta_{H_2}/R^5)$, where $Y = 9/4$ for $B_2$ symmetry, $Y = 3/4$ for $B_1$ symmetry, and $Y = -3$ for $A_1$ symmetry. The computed quadrupole moments are $\Theta_{Cd}(^3P) = -7.8$ a.u., $\Theta_{Cd}(^1P) = -18.0$ a.u., and $\Theta_{H_2} = 0.38$ a.u.

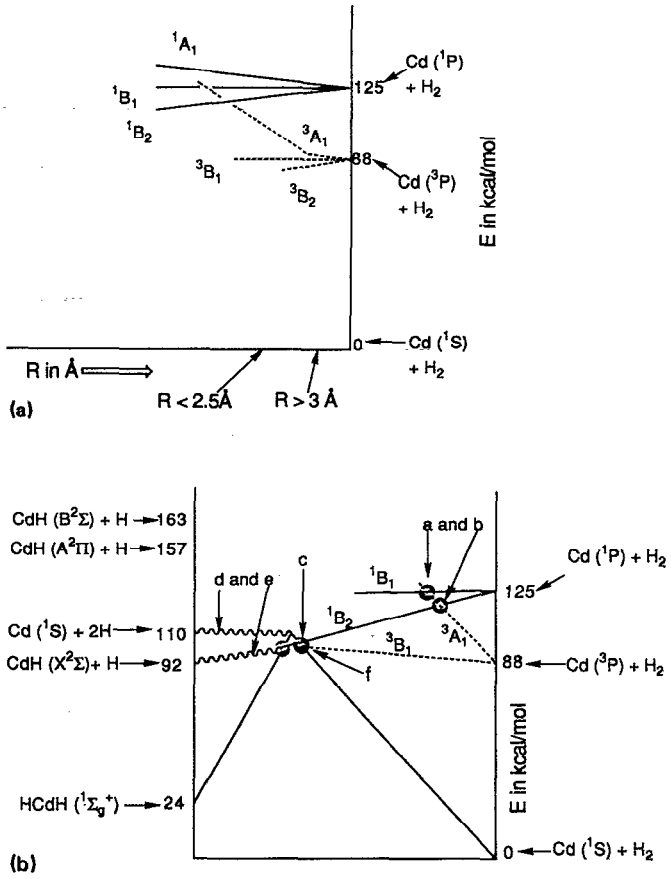


FIG. 1. (a) Qualitative energy-level diagram showing the behavior of the excited singlet and triplet states for large $R$ values; $R > 3$ Å characterizes the near-asymptotic region, and $R < 2.5$ Å is where chemical valence interactions become important (see Figs. 2 and 3). (b) Qualitative energy-level diagram showing primary surface intersections (marked by ●) that lead to various reaction products. All energies are in kcal/mol and are relative to the ground state of $Cd(^1S) + H_2$. The intersections labeled a and b may produce $^3P_J$ Cd via intersections of the $^1B_1$ (at $R = 2.0$ Å, $r = 0.9$ Å) and $^1B_2$ (at $R = 2.25$ Å, $r = 0.79$ Å) surfaces by the $^3A_1$ surface; c labels the $^1B_2$ and $^1A_1$ intersection that leads to formation of $^1S$ Cd + 2H via path d, and to $CdH(X\,^2\Sigma^+) + H$ via the $b_2$-mode instability path e; f labels the intersection of the $^1B_2$ and $^1A_1$ surfaces by the $^3B_1$ surface (near $R = 1.85$ Å, $r = 1.02$ Å) in the chemically reactive region.

## C. The surfaces at geometries where chemical valence forces are strong

In Fig. 1(b) we describe the *qualitative features of the* ground and lowest excited singlet and triplets PESs in the van der Waals region and the chemical-interaction region (which then connect to product channels). This presentation is not meant to provide a highly accurate representation of these three-dimensional PESs, but to help the reader view the relative energies and geometries of the various asymptotic states and most important surface intersections.

### 1. The lowest $^1A_1$ potential-energy surface

(a) *Global $C_{2v}$ picture at 1100 geometries.* The calculated lowest-energy $^1A_1$ potential-energy surface of $CdH_2$ is depicted in Fig. 2 as a function of $R$, the distance between the $H_2$ midpoint and the cadmium atom, and $r$, the H–H distance. A contour version of this same surface is given in Fig. 3. There are three asymptotic regions of interest in Figs. 2 and 3: the van der Waals minimum of the cadmium atom and $H_2$ molecule ($R = 4.4$ Å, $r = 0.76$ Å), the three separated cadmium and hydrogen atoms ($R = 4.4$ Å, $r = 3.5$ Å), and the linear H–Cd–H molecule ($R = 0.0$ Å, $r = 3.5$ Å). The total electronic energies (i.e., not including zero-point corrections) for these geometries are included in the data of Table I.

(b) *HCdH formation is endothermic.* Comparison of the energies of $Cd + H_2$ and H–Cd–H shows that formation of H–Cd–H (which was proven to be a local minimum by demonstrating that the Hessian matrix is positive definite) is *endothermic by 24.4 kcal/mol.* This is in contrast to the isovalent systems $Be + H_2$ and $B^+ + H_2$, where formation of the corresponding linear triatomic molecules is predicted (also at the CASSCF level of theory) to be exothermic by 23 (Ref. 18) and 47 (Ref. 17) kcal/mol, respectively. The harmonic vibrational frequencies of H $^{114}$CdH were found to be 540 (bending), 1620 (asymmetric stretch), and 1640 (symmetric stretch) $cm^{-1}$.

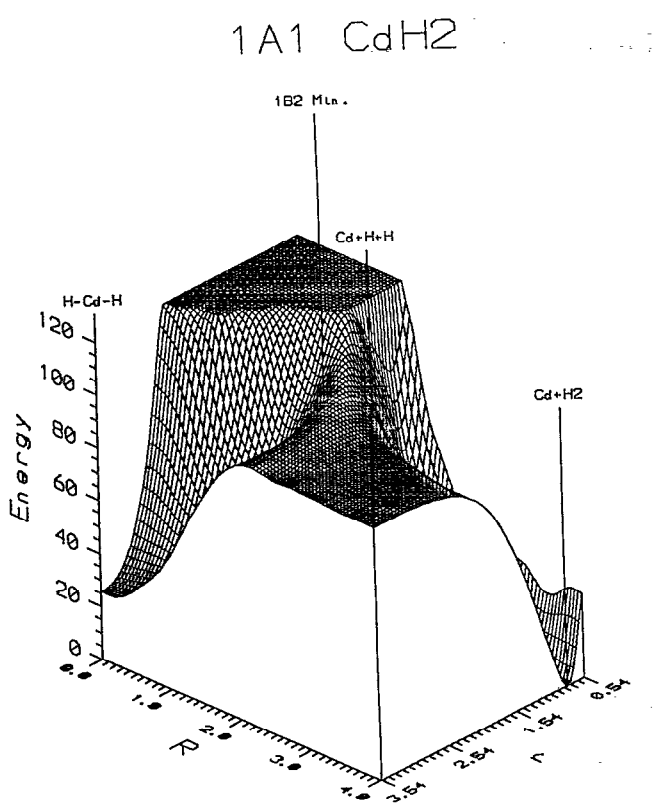


FIG. 2. The ground-state $^1A_1$ potential-energy surface. $R$ denotes the distance between the Cd atom and the $H_2$ midpoint and $r$ denotes the H–H distance. The point labeled "$^1B_2$ Min" indicates the geometry of the minimum on the $^1B_2$ surface.

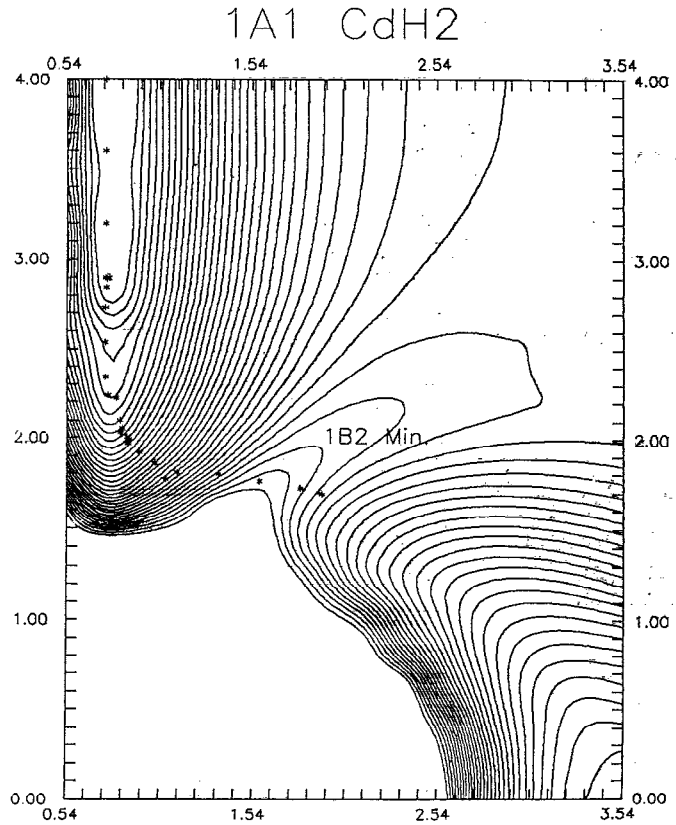


FIG. 3. Contour plot of the same surface shown in Fig. 2. $r$ is the horizontal axis and $R$ is the vertical axis (both in Å). The spacing between contours is 5 mhartrees (ca. 3 kcal/mol). The points marked by asterisks denote geometries in a streambed on the $^1B_2$ surface and the point labeled "$^1B_2$ Min" indicates the geometry of the minimum on this surface. The geometries that characterize the streambed on the $^1B_1$ surface (not shown here) closely parallel the asterisks.

(c) *There is no well-defined saddle leading from $Cd+H_2$ to HCdH.* Essential features of the $CdH_2$ $^1A_1$ PES shown in Figs. 2 and 3 are the two channels (one leading to linear H–Cd–H and the other to a cadmium atom and an $H_2$ molecule) which are divided by a ridge. Of particular interest is the lack of a stationary point along this ridge (apart from the asymptotic region corresponding to Cd + H + H). This, too, is in contrast to the $BeH_2$ and $B^+H_2$ systems, where a stationary point with an imaginary-frequency vibrational mode of $a_1$ symmetry connecting the two channels is observed. The lack of such a stationary point for $CdH_2$ implies that there is no saddle point for the direct insertion of Cd into the $H_2$ molecule, on the $^1A_1$ surface. Rather, the most energetically favorable means of insertion on this surface within this $C_{2v}$ symmetry is by initial dissociation of the $H_2$ molecule, followed by concerted addition of the two hydrogen atoms to cadmium.

### 2. The $^1B_1$ surface

Calculations on the weakly attractive (see Table III) $^1B_1$ state for $C_{2v}$ geometries have been carried out as a function of $R$, with the H–H distance $r$ optimized for each such $R$ value, to generate a "streambed" path. The energies of this

$^1B_1$ state along such a path, as well as the variations of $R$ and $r$, are described in Table IV.

The *geometries* lying in *this streambed closely parallel* those of the $^1B_2$ *surface streambed* from $R = 4$ Å in to $R = 2.1$ Å (compare the asterisks of Fig. 3 with the $R$, $r$ values of Table IV) although the energy variation of the $^1B_2$ state is much stronger than that of the $^1B_1$ state. *Past* $R = 2.1$ *Å*, the two *paths differ markedly*; the $^1B_2$ surface curves into the "chemically reactive" region where it intersects and couples strongly to the lowest $^1A_1$ state to produce CdH + H, HCdH, and Cd + 2H. In contrast, the $^1B_1$ *path remains "straight"* (i.e., with $r$ varying little from $r = 0.76$ Å) and *rather "flat" until* $R < 2.4$ *Å*, at which time it becomes quite repulsive; flux on this surface does not enter the chemically reactive region for the total energies appropriate here (125 kcal/mol).

In addition to characterizing the streambed on this $^1B_1$ surface, we found that, along this path, the repulsive $^3A_1$ *PES intersects it near* $R = 2.0$ *Å*, $r = 0.80$ *Å*, at which these surfaces lie ca. 10 kcal/mol *above* the $Cd(^1P) + H_2$ asymptote. See Fig. 4 where the $^1B_1$ surface and the underlying triplet surfaces are depicted along such a path. The (less-repulsive) $^3B_1$ surface lies ca. 38 kcal/mol lower at the $^1B_1$–$^3A_1$ crossing geometry. Addition of dispersion interaction terms to the $^1B_1$ energy could move this intersection point to somewhat longer $R$ values, thereby also moving its energy below the 10 kcal/mol value. Moreover, if we "shift" the entire $^3A_1$ curve upward to force the asymptotic $^1P$–$^3P$ splitting to be 126 − 88 = 38 kcal/mol rather than the calculated (see Table II 121 − 75 = 46 kcal/mol), the crossing point moves outward to only ca. 2.2 Å, at an energy that is still above the $^1B_1$ asymptote.

In summary, it seems likely that the $^3A_1$–$^1B_1$ intersection will occur for $R > 2.2$ Å and at energies somewhat above the $^1B_1$ state's asymptote. If any flux were to reach this crossing point, it could "hop" to the repulsive triplet surface and dissociate *to produce* $Cd(^3P_J) + H_2$.

### 3. The $^1B_2$ surface

Flux created on the $^1B_2$ excited state via photon excitation near the geometry of the ground-state van der Waals complex experiences strong forces that "drive" it along a *20 kcal/mol deep, narrow valley* streambed whose locus is depicted by the asterisks in Fig. 3. This path leads to the minimum (denoted 1B2 min in Figs. 2 and 3) on this $^1B_2$ surface at $R = 1.69$ Å and $r = 1.92$ Å and at an energy of 106 kcal/mol.

Along the path leading from the van der Waals geometry to the minimum, the $^1B_2$ *PES is intersected by the repulsive* $^3A_1$ *surface near* $R = 2.25$ *Å*, $r = 0.79$ *Å* (see Fig. 5), where the $^1B_2$ state's energy is ca. 3 kcal/mol below its asymptotic value (i.e., the "deep" chemically reacitve basin has not yet been entered). At this crossing point, flux can move onto the $^3A_1$ surface and dissociate *to produce* $^3P_J$ *Cd atoms*. At such geometries, the less-repulsive $^3B_1$ surface lies ca. 38 kcal/mol lower in energy.

Flux that progresses on the $^1B_2$ surface toward smaller $R$ values experiences a different fate. It moves on to approach the minimum on the $^1B_2$ surface, at which the lowest

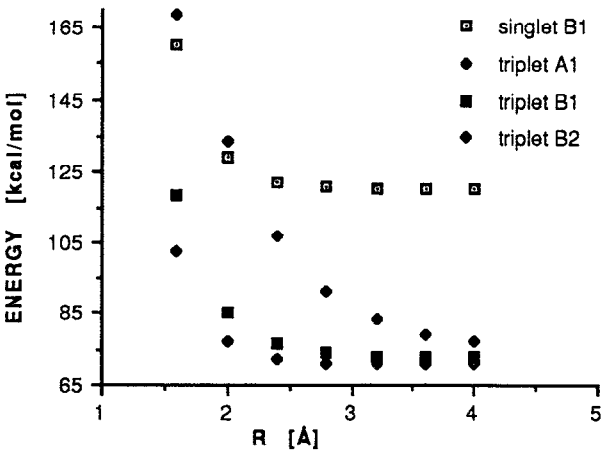


FIG. 4. Singlet–triplet crossings along the streambed of the $^1B_1$ state.

TABLE IV. Interaction energies on the $^1B_1$ surface.[a]

| $R$ (Å) | $r$[b] (Å) | $E$ (kcal/mol) |
|---|---|---|
| 1.6 | 0.7833 | 40 |
| 2.0 | 0.7655 | 10 |
| 2.4 | 0.7611 | 2 |
| 2.8 | 0.7579 | 1 |
| 3.2 | 0.7538 | 0 |
| 3.6 | 0.7545 | 0 |
| 4.0 | 0.7538 | 0 |

[a] Relative to the Cd + $H_2$ asymptote reported in Table II.

[b] For each $R$ value, the distance $r$ was varied to minimize the energy on this $^1B_1$ surface.

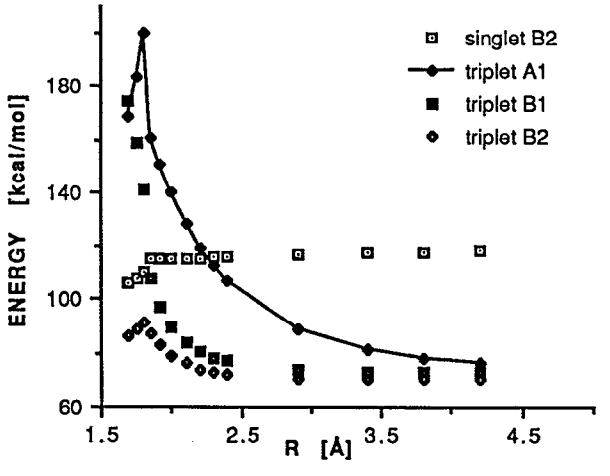


FIG. 5. Singlet–triplet crossings along the streambed of the $^1B_2$ state. The $^3A_1$ points have been connected by a curve to more easily follow the rapid change of energy that results from the "avoided crossing" discussed in the text.

$^1A_1$ surface is slightly (7 kcal/mol) lower in energy. At nearby geometries (e.g., where $R = 1.69$ Å and $r = 1.54$ Å), the $^1B_2$ surface lies 3.5 kcal/mol *below* the $^1A_1$ surface. Therefore, a $^1A_1$–$^1B_2$ *surface intersection seam* lies in this neighborhood of the ridge separating the Cd···$H_2$ and HCdH channels in Fig. 2, beginning near $R = 1.7$ Å, $r = 1.6$ Å and extending to smaller $R$ and smaller $r$ values. Flux encountering such intersection points can do either one of the following.

(i) Remain on the $^1B_2$ PES which, after passing below the $^1A_1$ surface, develops $b_2$-mode instability as a result of coupling to the higher-energy $^1A_1$ state as discussed in Sec. I F, thereby *generating* $CdH(X\,^2\Sigma^+) + H$.

(ii) "Hop" to the $^1A_1$ PES as the intersection is traversed, and subsequently move on to produce vibrationally "hot" HCdH, which can then *decompose to* $Cd + H + H$.

We also find that, in the neighborhood of the close approach and intersection of the $^1A_1$ and $^1B_2$ surfaces, the $^3B_1$ surface intersects near $R = 1.85$ Å, $r = 1.02$ Å (see Fig. 5); these intersections provide one more path to forming $Cd(^3P_J) + H_2$, for flux that enters this region and hops to the $^3B_1$ surface.

### 4. Treatment of $^1A_1$–$^1B_2$ nonadiabatic coupling to produce $b_2$-mode instability

Clearly, in the neighborhood of the close approach and intersections of the $^1B_2$ and $^1A_1$ surfaces discussed above, it is essential to verify the $b_2$-mode instability (or lack thereof) of each of these surfaces. To examine the $b_2$-mode stability of the $^1B_2$ state at its own minimum, we proceeded as follows:

(i) Because the GAMESS program cannot compute analytical second energy derivatives, we introduced a small (0.005 29 Å) asymmetric distortion of the two Cd–H bond lengths.

(ii) After which the CASSCF energy of the lowest-energy singlet state (the $^1A_1$ state lies ca. 7 kcal/mol lower here) was evaluated.

(iii) First, a CASSCF calculation on the lower-lying $^1A_1$ state was performed, and the negative curvature on this $^1A_1$ surface was verified via the small $b_2$-mode distortion noted above.

(iv) Second, a state-averaged CASSCF process, in which the $^1A_1$ and $^1B_2$ states are equally weighted in the energy functional being optimized, was performed and the energy of the resulting $^1A_1$ state was examined under the small $b_2$-mode distortion to again verify its negative curvature.

The results of both such calculations were the same: the $^1A_1$ state is unstable with respect to $b_2$-mode motions at the geometry where the $^1B_2$ state has its minimum but lies above the $^1A_1$ state. Likewise, the $^1B_2$ state will be $b_2$-mode unstable when it has intersected and now lies below the $^1A_1$ state. We thought it prudent to carry out both sets of CASSCF calculations because the former, which optimizes orbitals and configuration mixing coefficients for the $^1A_1$ state, differentially stabilizes the $^1A_1$ state relative to the $^1B_2$ state. On the other hand, the state-averaged CASSCF calculation probably underestimates the energy gap between the two states. Because the strength of coupling, as given by the formula in Sec. I F, depends strongly on this energy gap, it was important to verify the negative $b_2$-mode curvature for situations in which this gap is overestimated and underestimated.

### 5. The $^3B_2$ and $^3\Sigma^+$ surfaces and relation to full-collision experiments

We found the $^3B_2$ and $^3\Sigma^+$ surfaces to display behavior that may be useful in interpreting earlier "full-collision" experiments[11,12] in which $^3P_1$ Cd atoms were allowed to collide with $H_2$ molecules and $CdH(X\,^2\Sigma^+) + H$ products were detected.

In particular, the $^3B_2$ surface, which was not discussed in earlier sections since its PES does not intersect the $^1B_2$ or $^1B_1$ surfaces in regions where flux in the half-collision experiments is likely to flow, has been found to (i) be attractive in the van der Waals region as noted earlier, and (ii) to have a *minimum* at $R = 1.70$ Å, $r = 2.12$ Å whose energy lies *8 kcal/mol above* our computed $Cd(^3P) + H_2$ *asymptote*.

These two facts imply that there must be a minimum on the $^3B_2$ potential surface at long range (probably in the van der Waals region), separated by a transition state that connects to the minimum at $R = 1.70$ Å, $r = 2.12$ Å. We found such a *transition state* to occur at $R = 1.84$ Å, $r = 1.28$ Å and to have an energy of 92 kcal/mol. The transition state is visible in Fig. 5 (because the streambed paths on the $^1B_2$ and $^3B_2$ surfaces are quite similar for $R >$ ca. 1.8 Å).

It should also be noticed in Fig. 5 that the energy of the $^3A_1$ state falls drastically near $R = 1.8$ Å as the result of an avoided crossing between the $1a_1^2 2a_1 3a_1$ and $1b_2^2 1a_1 2a_1$ configurations. We speculate that the second-order Jahn–Teller coupling discussed in Sec. I F, and now applied to the $^3A_1$ and $^3B_2$ states, causes negative $b_2$-mode curvature on the (lower-lying) $^3B_2$ surface and opens the $CdH(X\,^2\Sigma^+) + H$ channel for $R < 1.7$ Å with a $^3B_2$-state energy between 8 and 14 kcal/mol above the $Cd(^3P) + H_2$ asymptote.

Another possibility to produce $CdH(X\,^2\Sigma^+) + H$ in the "full-collision" experiments comes through the $^3\Sigma^+$ surface. Even though the colinear paths are less probable than the $C_{2v}$ paths, we considered this option in view of the activation barrier detected on $^3B_2$ surface in $C_{2v}$ geometry. On the $^3\Sigma^+$ surface we also found a transition state which lies at 102 kcal/mol [i.e., even higher than the $^3B_2$ transition state (see Table 1)].

In conclusion, we expect an activation barrier for the $Cd(^3P) + H_2 \Rightarrow CdH(X\,^2\Sigma^+) + H$ reaction. Earlier full-collision data indeed demonstrate that this reaction, which is essentially thermoneutral, proceeds with a nonzero activation.[11,12]

## IV. CONCLUSIONS AND SUMMARY OF FINDINGS

This paper has attempted to provide a more detailed understanding of the reaction dynamics of $^1P$ cadmium with the ground-state hydrogen molecule. At the energy of $^1P$ $Cd + H_2$ [ca. 125 kcal/mol above ground-state $Cd(^1S) + H_2$ reactants], it is possible to access products via the ground-state $^1A_1$ surface (i.e., $HCdH(^1\Sigma_g^+)$ at 24 kcal/mol and $Cd(^1S) + H + H$ at 110 kcal/mol) or products

that require $b_2$-mode instability to occur somewhere along the path from $^1P$ Cd + $H_2$ (i.e., $CdH(^2\Sigma^+) + H$ at 92 kcal/mol). Of course, quenching to produce $Cd(^3P_J) + H_2$ at 88 kcal/mol is also energetically possible. Formation of $CdH(A\,^2\Pi) + H$ or $CdH(B\,^2\Sigma) + H$ is *not* energetically possible.

*To explain* the formation of $CdH(X\,^2\Sigma^+) + H$, we propose the following. (i) Flux starts on the excited $^1B_2$ electronic state and (ii) moves under strongly attractive forces to a region where the $^1B_2$ surface penetrates the lowest $^1A_1$ surface (see Figs. 2 and 3 for an example of such a region), (iii) where asymmetric ($b_2$-mode) instability *on this* $^1B_2$ *surface* is induced by the presence of the nearby but higher-lying $^1A_1$ surface, (iv) as a result of which distortion along this $b_2$ mode and hence dissociation to $CdH(^2\Sigma^+) + H$ products occurs from the $^1B_2$ surface.

It is also possible that flux "hops" to the $^1A_1$ surface, and evolves on this surface to geometries where this $^1A_1$ surface lies just below the $^1B_2$ PES, at which point $b_2$-mode instability will occur *on the* $^1A_1$ *surface*, thereby allowing $CdH(^2\Sigma^+) + H$ products to be formed from this $^1A_1$ surface.

*To explain* the formation of Cd + H + H, we propose the following. (i) Flux starts on the excited $^1B_2$ electronic state and again moves to a region where the $^1B_2$ and $^1A_1$ surfaces approach one another, (ii) at which time the flux can "hop" to the underlying $^1A_1$ state, either through an intersection of the two surfaces or via nonadiabatic coupling mediated by an asymmetric vibration, (iii) after which the flux moves "downhill" directly into the HCdH potential well (with ca. 125 − 24 = 101 kcal/mol of internal vibrational energy) on this $^1A_1$ surface, (iv) from which it has enough energy to escape and produce $Cd(^1S) + H + H$.

*To explain* the formation of $Cd(^3P_J) + H_2(X\,^1\Sigma_g^+)$, we find that both the $^1B_1$ and $^1B_2$ surfaces may be involved. In these cases, we propose the following.

(i) Flux prepared on the $^1B_1$ or $^1B_2$ surface is moved by attractive forces (weak in the former case, and strong in the latter) from $R = 4$ Å inward (toward $R = 2.0$–$2.2$ Å, $r = 0.77$ Å for the $^1B_1$ surface and to $R = 2.25$ Å, $r = 0.79$ Å for the $^1B_2$ surface) to where the repulsive $^3A_1$ PES crosses from below.

(ii) The crossing point ($R = 2.0$–$2.2$ Å, $r = 0.8$ Å) for the $^1B_1$ surface may lie *above* the $Cd(^1P) + H_2$ asymptote (it is difficult for us to determine this precisely due to the restricted treatment of the electron correlation and neglect of spin–orbit coupling), so this point may not easily be accessed (without tunneling) by flux on the $^1B_1$ PES.

(iii) However, the $^3A_1$–$^1B_2$ crossing ($R = 2.25$ Å, $r = 0.79$ Å with an energy ca. 3 kcal/mol below the $Cd(^1P) + H_2$ asymptote) is accessible, and flux can hop onto the $^3A_1$ surface and dissociate to yield $Cd(^3P_J) + H_2$.

(iv) Flux that remains on the $^1B_2$ surface past this intersection with the $^3A_1$ PES has another chance to produce $Cd(^3P_J) + H_2$ because the $^1B_2$ surface is intersected by the $^3B_1$ PES in the chemically reactive region (near $R = 1.85$ Å, $r = 1.02$ Å) where close approach of the $^1A_1$ and $^1B_2$ PESs occurs.

## ACKNOWLEDGMENTS

This work was supported through National Science Foundation Grant No. CHE 881475 and by The Office of Naval Research. The authors would like to acknowledge several enlightening and stimulating discussions with our colleague, Professor W. Breckenridge.

[1] I. Wallace, D. J. Funk, J. G. Kaup, and W. H. Breckenridge, in *Gas Phase Metal Reactions*, edited by A. Fontijn (Elsevier, Amsterdam, in press).
[2] W. H. Breckenridge, O. Benoist d'Azy, M. C. Dauval, C. Jouvet, and B. Soep, in *Stochasticity and Intramolecular Redistribution of Energy*, edited by R. Lefebvre and S. Mukamel (Reidel, Dordrecht, 1987).
[3] W. H. Breckenridge, Acc. Chem. Res. **22**, 21 (1989).
[4] M.-C. Duval, B. Soep, and W. H. Breckenridge, J. Phys. Chem. **95**, 7145 (1991).
[5] D. J. Funk and W. H. Breckenridge, J. Chem. Phys. **90**, 2927 (1989).
[6] W. H. Breckenridge, C. Jouvet, and B. Soep, J. Chem. Phys. **84**, 1443 (1986).
[7] I. Wallace, J. G. Kaup, and W. H. Breckenridge, J. Phys. Chem. **95**, 8060 (1991).
[8] I. Wallace, J. D. Funk, and W. H. Breckenridge (unpublished).
[9] I. Wallace and W. H. Breckenridge (unpublished).
[10] W. H. Breckenridge, W. L. Nikolai, and D. Oba, J. Phys. Chem. **90**, 5724 (1986).
[11] W. H. Breckenridge, H. Umemoto, and J-H. Wang, Chem. Phys. Lett. **123**, 23 (1986).
[12] M. Giroud and O. Nedelec, Chem. Phys. Lett. **152**, 167 (1988).
[13] N. Adams, W. H. Breckenridge, and J. Simons, Chem. Phys. **56**, 327 (1981).
[14] R. P. Blickensderfer, K. D. Jordan, N. Adams, and W. H. Breckenridge, J. Phys. Chem. **86**, 1930 (1982).
[15] D. O'Neal, H. Taylor, and J. Simons, J. Phys. Chem. **88**, 1510 (1984).
[16] A. Bernier and P. Millie, J. Chem. Phys. **88**, 4843 (1988).
[17] J. Nichols, M. Gutowski, S. J. Cole, and J. Simons, J. Phys. Chem. **96**, 644 (1992).
[18] M. Gutowski, G. Chalasinski, S. Cole, and J. Simons (unpublished).
[19] J. A. Boatz, K. L. Bak, and J. Simons, Theor. Chim. Acta (in press).
[20] J. Simons, *Energetic Principles of Chemical Reactions* (Jones and Bartlett, Boston, 1983).
[21] P. J. Hay, and R. J. Wadt, J. Chem. Phys. **82**, 270 (1985).
[22] J. S. Binkley, J. A. Pople, and W. J. Hehre, J. Am. Chem. Soc. **102**, 939 (1980).
[23] (a) M. Dupuis, D. Spangler, and J. J. Wendoloski, National Resource for Computations in Chemistry Software Catalog, University of California, Berkeley, CA (1980), Program QG01; (b) M. W. Schmidt, K. K. Baldridge, J. A. Boatz, J. H. Jensen, S. Koseki, M. S. Gordon, K. A. Nguyen, T. L. Windus, and S. T. Elbert, QCPE Bull. **10**, 52 (1990).
[24] The Utah MESS-KIT is a suite of highly modular codes that were programmed in-house to give a variety of electronic structure functionalities by J. A. Nichols, M. R. Hoffman, R. A. Kendall, H. L. Taylor, D. W. O'Neal, E. Earl, R. Hernandez, M. Gutowski, J. A. Boatz, K. L. Bak, J. L. Anchell, X. Wang, M. Feyereisen, and J. Simons.
[25] W. H. Miller, N. C. Handy, and J. E. Adams, J. Chem. Phys. **72**, 99 (1980).
[26] C. E. Moore, *Atomic Energy Levels* Natl. Stand. Ref. Data Ser. Natl. Bur. Stand. (U.S. GPO, Washington, DC, 1971), Vols. 1 and 3.
[27] K. P. Huber and G. Herzber, *Molecular Spectra and Molecular Structures, IV. Constants of Diatomic Molecules* (Van Nostrand Reinhold, New York, 1979).
[28] P. Pyykko, J. Chem. Soc. Faraday Trans. 2 **75**, 1256 (1979).
[29] S. F. Boys and F. Bernardi, Mol. Phys. **19**, 553 (1970).